Journal of Engineering Science and Technology
Vol. 15, No. 2 (2020) 894 - 904

EFFECT OF SONICATION TIME AND PARTICLE SIZE FOR SYNTHESIS OF MAGNETIC NANOPARTICLE FROM LOCAL IRON SAND

NUR ROFIQOH EVIANA PUTRI[1], SALSABILA ISNA FIRDAUSI[1], MAZAYA NAJMINA[2], SHINTA AMELIA[3], DANIEL TIMOTIUS[1], YUNI KUSUMASTUTI[1,4,*], HIMAWAN TRI BAYU MURTI PETRUS[1,5]

[1]Chemical Engineering Department, Universitas Gadjah Mada,
Jl. Grafika No 2, 55281 Yogyakarta, Indonesia
[2]Department of Materials Science and Engineering,
Graduate School of Pure and Applied Sciences, University of Tsukuba,
1-1-1 Tennodai, 305-8577 Tsukuba, Japan
[3]Department of Chemical Engineering, Universitas Ahmad Dahlan,
Jl. Prof. Dr. Soepomo, Janturan, Umbulharjo 55164, Yogyakarta, Indonesia
[4]Bioresource Engineering Group, Universitas Gadjah Mada,
Jl. Grafika No 2, 55281 Yogyakarta, Indonesia
[5]Sustainable Mineral Processing, Universitas Gadjah Mada,
Jl. Grafika No 2, 55281 Yogyakarta, Indonesia
*Corresponding Author: yuni_kusumastuti@ugm.ac.id

Abstract

In this research, iron sand from local resource was used to synthesis the Fe_3O_4 nanoparticle. Effects of sonication time and a different size of iron sand were analysed in the preparation process to obtain magnetic nanoparticle, which has excellent properties. The black colour of obtained magnetic nanoparticle was further analysed with the Brunauer-Emmett-Teller (BET) method to observe the porous structure of materials, including surface area, average pore diameter, and the type of pore size. The results show that the produced magnetic nanoparticles have a mesoporous structure with the average pore diameter ranged within 3.594-5.392 nm. This mesoporous architecture is desired in drug delivery application for high drug loading. Scanning Electron Microscopy (SEM) and Transmission Electron Microscopy (TEM) result shows that the magnetic nanoparticles have homogeneous spherical shape and nano in size. Such nanoparticle can be easily transferred in the body through the blood and enhance the targeting ability. Meanwhile, Energy Dispersive X-Ray (EDX) result shows that the major element found in MNP samples are iron and oxygen, which could form iron oxides. Thus, the resulted Fe_3O_4 nanoparticle from local iron sand could be used as an alternative approach as a biomaterial for cancer treatment.

Keywords: Biomaterial, Iron sand, Nanomagnetic.

1. Introduction

Nanomaterials become an interest for last decade, especially in the biomedical field. One of the promising nanomaterials, which widely developed for cancer treatment is magnetic nanoparticle [1]. Magnetic nanoparticle (MNP) can be bound with drug or other biomolecule agents, transferred to the body, then accumulated in the targeted cancer cells by inducing a magnetic field using an implanted magnet or applied field [1].

Thus, the targeting ability of a drug can be increased. Their magnetic properties can be used for several applications, such as magnetic resonance imaging (MRI) [2] and hyperthermia therapy [3]. In the first biomedical application proposal, MNP can be delivered through the blood and targeted in a specific part of the body by using the magnetic field [4]. The heat will be generated in the targeted tissue and kill the tumour cells [5].

MNP can be modified using different materials, which can carry cancer drug and increase their loading. Lengert et al. [6] conducted research, which loaded MNP into a hollow silver hydrogel microsphere. The results showed that prime loading capacity was obtained when the outer shell layer of microsphere was adsorbing MNP. It could also act as stimuli to enhance the drug targeting ability. Thus, by using magnetic nanoparticle, the effectiveness of cancer therapy can be increased due to the dual function of MNP, which can act as a drug carrier and also as hyperthermia agent.

Several studies have been done to produce Fe_3O_4 nanoparticle from commercial iron. Yallapu et al. [7] have successfully synthesized iron oxide nanoparticle from commercial Iron (III) and Iron (II) using precipitation method and loaded curcumin into the materials using the diffusion method. The result exhibited magnetic nanomaterial with 9 nm-sized individual particle grain and 123 nm aggregative particle size. It also showed superior magnetic resonance imaging properties and raised the targeting ability of curcumin.

Another research was conducted by Jain et al. [8], which produced magnetic nanoparticle with dual functional properties, as drug delivery materials and magnetic resonance imaging. They prepared the materials by co-precipitation of commercial Fe (III) and Fe (II) with ammonium hydroxide, then coated with oleic acid. The obtained modified magnetic nanoparticles were loaded with doxorubicin (DOX) and paclitaxel (PTX) drug to see the drug loading and release ability. Their research resulted in nano-sized materials with the core particle size of 10-25 nm and mean hydrodynamic diameter was in the range of 210-250 nm. The drug loading capacity was high with the efficiency of DOX and PTX loading were 82% and 95%, respectively.

In the present research, Fe_3O_4 will be synthesized from local iron sand, which is abundantly available. Rahmawati et al. [9] have successfully synthesized Fe_3O_4 nanoparticle from local iron sand using different frequency and stirring rate of ultrasonic irradiation. However, there is still limited research that has been done using ultrasonic irradiation method. Therefore, more study is needed to optimize the process. This research aims to study the effect of different iron sand size and reaction time during ultrasonic radiation process, which could affect the properties of the resulted MNP.

2. Materials and Methods

2.1. Materials

The iron sand was obtained from Glagah Beach, Special Region of Yogyakarta (S7°54'45.8" E110°3'59.5"). Hydrochloric acid (HCl) (37% Purity Merck, Germany), ammonium hydroxide solution (NH_4OH) (30% Purity Merck, Germany), ethanol absolute (Merck, Germany) and distilled water were used during the synthesizing process.

2.2. Methods

2.2.1. Preparation of magnetic nanoparticle

Magnetite was extracted from Kulonprogo's iron sand by using a magnetic separator. The extracted magnetite was sieved using different size of mesh screens as shown in Table 1. Ten grams of magnetite particles were dispersed in 54 mL of 12 M HCl (37%) and left for ultra-sonication with different radiation time as shown in Table 1 using sonicator bath at room temperature. The frequency used in this process was 30 kHz based on the equipment specifications.

The suspension solution was filtered using a 0.8 μm filter paper to obtain $FeCl_2$ and $FeCl_3$ solution. Approximately ±50 mL of 6.5 M NH_4OH solution was added to the filtered solution one drop at a time until the black-coloured deposit was formed. The deposit was washed repeatedly with ethanol and distilled water until neutral pH is reached. After that, the deposit was separated from the solution by centrifugation, dried in an oven at a temperature of 60°C for ±12 hours, and then collected with a magnet.

Table 1. Sample of magnetic nanoparticle.

Sample	Size of mesh screen (mesh)	Ultra-sonication time (minutes)
MNP1	70	30
MNP2	140	30
MNP3	140	120

2.2.2. Characterization

Brunauer-Emmett-Teller (BET) Nova 2000, Quantachrome (USA) was used to analyze the characterization of pore size. In this study, BET will be used to determine surface area and type of isotherm of produced MNP. Meanwhile, the Barret-Joyner-Halenda (BJH) method will be used to determine the pore types. The adsorption-desorption N_2 curve could exhibit different types of pores. Adsorbed volume (cc/g) is plotted in the different relative pressure.

X-Ray Diffraction (XRD) by Rigaku Miniflex 60 (Japan) was used to analyze the crystal size and structure of the obtained magnetic nanoparticles. The analysis was done by using Cu Kα X-Ray source with wavelength number set at 0.1540 nm operated in 40 kW.

Transmission Electron Microscopy (TEM) JEOL JEM-1400 (USA) was used for morphological analysis of the nano-magnetite surface so that the size of the nanoparticle can be analysed.

Scanning Electron Microscopy-Energy Dispersive X-Ray Spectroscopy (SEM-EDX) Hitachi models SU-3500 (Japan) was used for morphological analysis of the nano-magnetite surface. In addition, SEM-EDX can also be used to determine the element of sample.

3. Results and Discussion

3.1. Brunauer-Emmett-Teller (BET) analysis

Iron sand, which has been modified into a magnetic nanoparticle was then characterized using Brunauer-Emmett-Teller (BET) analysis. The surface area of the samples can be seen in Table 2. Magnetic nanoparticles with the same mesh size but different sonication times show different results of surface area. During sonication of 30 minutes, the produced magnetic nanoparticle has a surface area of 183.194 m^2/gram and average pore diameter of 5.392 nm while magnetic nanoparticle with 2 hours sonication time has a surface area of 273.301 m^2/gram and average pore diameter of 3.608 nm.

This result shows that the magnetic nanoparticle with 2 hours sonication time has a greater surface area than magnetic nanoparticle with 30 minutes sonication time. It is because the longer sonication time indicates the longer precipitation process, which resulted in the stronger disintegration of solid particles into the solution, which tends to make a great reduction of particle size. Thus, the surface area was increased as the consequences of the reduction of particle size. This phenomenon is similar to the formation of nanoparticles by emulsification process [10]. In addition, Table 2 shows that magnetic nanoparticles with the same sonication time but different particle sizes produced different surface areas and pore diameter. By using 140 mesh of iron sand size, the surface area of obtained magnetic nanoparticle was 183.194 m^2/gr and the pore diameter average was 5.392 nm. Meanwhile, when using 70 mesh iron sand size, the magnetic nanoparticle surface area was 297.093 m^2/gram and a pore diameter average was 3.594 nm. This shows that larger particle size leads to smaller average pore diameter. The desired pore diameter is in the range of 2-50 nm, according to IUPAC classification for mesoporous materials.

Table 2. Magnetic nanoparticle characterization.

Characterization	Specific surface area (S_{BET}), (m^2/g)	Average pore diameter (nm)
MNP1	297.093	3.594
MNP2	183.194	5.392
MNP3	273.301	3.608

Furthermore, the pore size distribution on the magnetic nanoparticle can also be determined from the type of isothermic equilibrium curve achieved from the sample. The adsorption equilibrium condition is a condition when the adsorption rate is the same as the desorption rate. After the adsorption process on the adsorbent surface lasted long enough, the gas is absorbed on the adsorbent and the gas in the gas body will reach equilibrium conditions. In evaluating the adsorption data, the right isotherm equation is needed to be used for this type of adsorption system. Through the isothermic equilibrium curve, the amount of adsorbate absorbed on the adsorbent can be determined.

Based on IUPAC classification, the type of isotherm curve produced using Barret, Joyner and Halenda (BJH) methods for magnetic nanoparticles is type IV [11]. The isotherm curve with this type is in the relatively low to medium pressure range. At a certain pressure range, the desorption line does not coincide with the adsorption line (hysterical phenomenon). Lines that do not coincide between adsorption and desorption lines indicate adsorbents with mesoporous size. In addition, the average pore diameter of all samples from BET analysis is in the range of 3.594 to 5.392 nm, which fulfil the criteria of mesoporous material based on IUPAC nomenclature. The mesoporous size of nanoparticle is needed for drug delivery application to increase the drug loading.

The equilibrium curve for magnetic nanoparticles can be seen in Fig. 1. Figure 1 shows that all samples of magnetic nanoparticles exhibit a typical isothermic of type-IV curves with the hysteresis loop of H3 [12]. The hysteresis loop exists at the relative pressure between 0.4 to 1.0; 0.2 to 0.9; and 0.4 to 0.9 for MNP1, MNP2, and MNP3 samples respectively and indicates the existence of mesoporous structure [12]. Such loops would not exist in non-mesoporous architecture [13, 14]. This result was also similar to the previous study on mesoporous particles, which studied based on the isotherm curve [15]. The direct synthesis of mesoporous architecture, which does not use any surfactant was explored before [16]. The mesoporous structure is formed due to the agglomeration of individual nanoparticles affected by pH, the nature of alkali, the rate of alkaline solution addition and also the drying process [16].

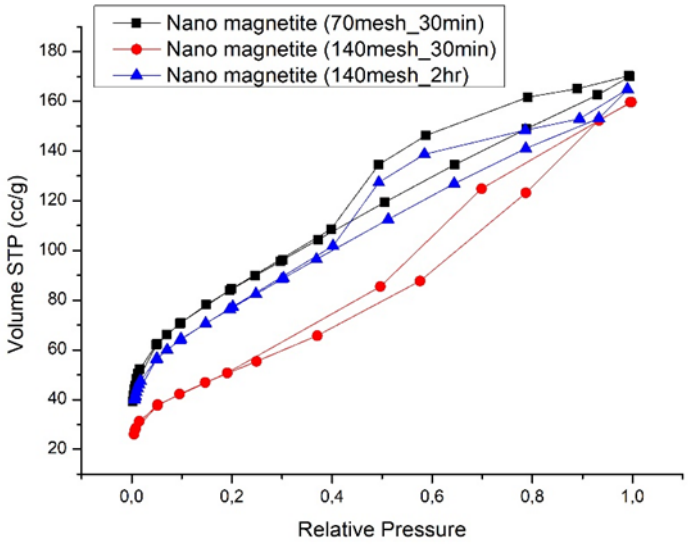

Fig. 1. Isotherm magnetic nanoparticle curve.

At the same relative pressure, the nano-sized mesh curve with a size of 70 mesh produces a larger pore volume than the nano-magnetic curve with a size of 140 mesh. Based on this, it can be concluded that the larger iron sand size, the greater pore volume will be obtained, therefore, it can increase drug loading [17]. In addition, Fig. 1 also shows that different sonication times gave different results of the isothermic curve trend. The comparison of the curve of MNP2 samples (140

mesh size with 30 minutes sonication time) with MNP3 samples (140 mesh curve with 120 minutes sonication time) shows that longer sonication time produced a larger volume. It is because the longer sonication time could enhance the elucidation of solid particles into the solution, which tends to make a great reduction of particle size. Thus, the total volume was increased.

3.2. X-Ray Diffraction (XRD) analysis

XRD graph exhibits the crystal structure of samples. Figure 2 showed that all of the samples have the characteristic peaks of Fe_3O_4 as assigned according to JCPDS card no. 19-0629 with miller index of (2 2 0), (3 1 1), (4 0 0), (5 1 1), and (4 4 0), respectively [18].

The crystallite size of magnetic nanoparticles was determined using Scherer equation [19]:

$$D = \frac{k\lambda}{\beta \cos\theta} \quad (1)$$

where D is crystallite size (nm); k is shape parameter (0.89 for magnetite); λ is the X-ray wavelength (0.154 rad); β is full width at half maximum (FWHM), and θ is the corresponding Bragg angle. Based on Eq. (1), the calculated crystallite size are 68.8, 3.7, and 2.7 for MNP1, MNP2, and MNP3 samples, respectively. As the larger iron sand size, the crystallite size of nanoparticle increases.

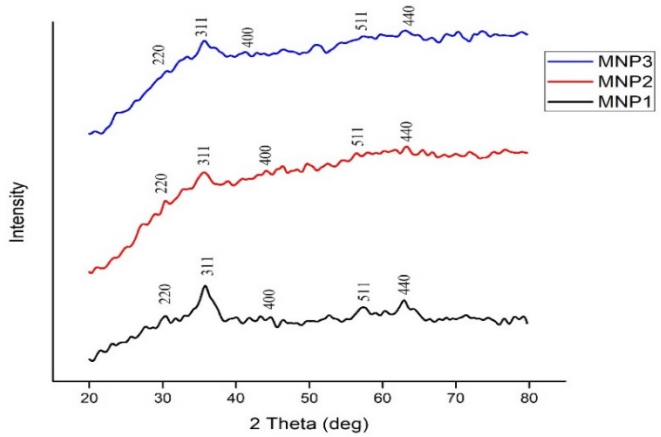

Fig. 2. The pattern of X-Ray diffraction of nanomagnetic samples.

3.3. Transmission Electron Microscopy (TEM) analysis

TEM characterization was used to determine the morphological structure of magnetic nanoparticles. It is expected that the produced nanoparticle magnetic has a homogeneous and nanometer-sized structure, which less than 100 nm. Figure 3 shows the result of TEM analysis of MNP2 sample. The result shows that resulted MNP has a nano-sized structure, which is good for biomedical application. The particles have a similar size with biomolecules, which provoke better intracellular uptake compared to the micron-size materials. It is because nano-size material

could facilitate better penetration into capillaries and through fenestrations. They can easily access many areas of the body through the circulating system and provide better drug delivery precisely for cancer cells [17]. They also can modify with multiple targeting moieties such as peptides or antibodies for effective cancer-targeting [20]. Thus, the effectiveness of cancer cell treatment can be increased.

Figure 3 also shows that the obtained Fe_3O_4 formed nearly spherical shaped-particle and tends to make agglomeration. The agglomeration phenomenon is caused by particle interaction, which usually possessed by magnetic materials called DLVO theory. It explains that the agglomeration of aqueous dispersions was determined by a repulsive force between the charged particles [21]. In addition, the rise of surface free energy resulted from the decrease of magnetic size also tends to form agglomeration [22]. In addition, the absence of surfactant enhances the formation of aggregates of this particle. Such phenomenon determines the stability suspension of magnetic nanoparticles in the liquid medium [16].

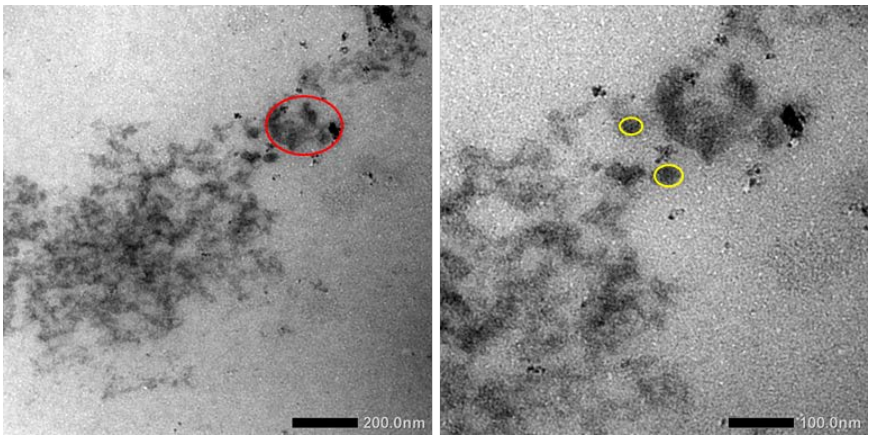

Fig. 3. TEM analysis of MNP2 sample. Left side indicates the TEM image in lower magnification, meanwhile, the right side indicates the TEM images in higher magnification. Redline shows the agglomeration of nanomagnetic, and the yellow line shows spherical shape of individual nanomagnetic.

3.4. Scanning Electron Microscopy-Energy Dispersive X-Ray Spectroscopy (SEM-EDX) analysis

The next magnetic nanoparticle characterization is Scanning Electron Microscopy (SEM). Figure 4 is the result of SEM from the three magnetic nanoparticle samples. Based on Fig. 4, it can be seen that the three produced magnetic nanoparticles tend to agglomerate. However, MNP3 shows more homogeneous distribution compared to MNP1 and MNP2. It is because MNP3 sample was synthesized using longer sonication time and smaller iron sand size, which provoke better dispersion process. Thus, it resulted in more homogeneous nanoparticle formation.

The result of Energy Dispersive X-Ray Spectroscopy (EDX) analysis shows that some impurities in iron sand can be reduced during MNP synthesis process. The composition of each component in each sample can be seen in Table 3.

Another research using different method could get iron oxide nanoparticle without any impurities [23]. More purification is needed to obtain such particle after co-precipitation method. Table 3 shows the major component of three magnetic nanoparticle samples, which are iron and oxygen, which could form iron oxide. Based on XRD data, the obtained iron oxide was iron oxide II nanoparticle. However, the small amount of *C*l also appears. The Cl detected was the result of the residual hydrochloric acid used during the synthesis process.

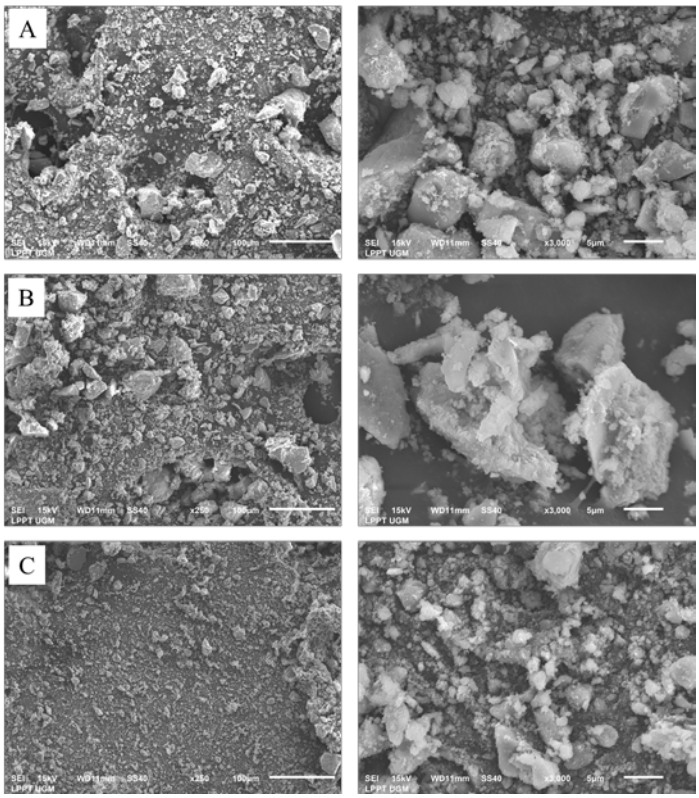

Fig. 4. SEM analysis of magnetic nanoparticle of: a) MNP1, b) MNP2 and c) MNP3 samples. Left column indicates the SEM images in low magnification, while right column indicates the SEM images in high magnification.

Table 3. Magnetic nanoparticle composition.

Element	Mass (%)			
	Iron sand	**MNP1**	**MNP2**	**MNP3**
O	43.18	38.15	42.54	34.40
Na	0.92	-	-	-
Mg	1.43	-	-	-
Si	6.43	-	-	-
Ca	0.70	-	-	-
Cl	-	2.79	1.55	2.52
Ti	3.78	5.92	4.70	5.88
Fe	43.55	53.02	51.21	57.20
Total	**100.00**	**100.00**	**100.00**	**100.00**

4. Conclusions

Utilization of local iron sand to produce magnetic Fe_3O_4 nanoparticle using ultrasonic radiation method was studied. By varying the size of iron sand (140 mesh and 70 mesh) and ultra-sonication time (30 minutes, 120 minutes), optimization was done. Further characterization was then used to see their effect on pore properties, morphology, and also the metal content of the samples. Results show that samples using 140 mesh iron sand and 120 minutes ultra-sonication time produce nanomaterial with high surface area and mesoporous type of pores, which is good for drug delivery application. SEM and TEM images also show that the samples produce a homogeneous spherical shape with nanometre ranged size, while the EDX results show that the obtained MNP has higher Fe content compared to the iron sand. From the results, it can be concluded that Fe_3O_4 nanoparticle from Glagah Beach, Special Region of Yogyakarta is potential to be used in drug delivery system.

Acknowledgement

The authors acknowledge Universitas Gadjah Mada's internal grant scheme "Modifikasi Mesoporous Nanosilica dengan Magnetic Nanoparticle Berbasis Pasir Besi Kulonprogo sebagai Drug Carrier dalam Terapi Hipertermia pada Kanker" with research grant number 3160/UN1/DITLIT/DIT-LIT/LT/2018.

Abbreviations

BET	Brunauer-Emmett-Teller
BJH	Barret-Joyner-Halenda
DOX	Doxorubicin
EDX	Energy Dispersive X-Ray
HCl	Hydrochloric Acid
IUPAC	International Union of Pure and Applied Chemistry
JCPDS	Joint Committee on Powder Diffraction Standards
MNP	Magnetic Nano Particle
MRI	Magnetic Resonance Imaging
NH_4OH	Ammonium Hydroxide Solution
PTX	Paclitaxel
SEM	Scanning Electron Microscopy
TEM	Transmission Electron Microscopy
WHO	World Health Organization
XRD	X-Ray Diffraction

References

1. Arruebo, M.; Fernandez-Pacheco, R.; Ibarra, M.R.; and Santamaria, J. (2007). Magnetic nanoparticles for drug delivery. *Nano Today*, 2(3), 22-32.
2. Cunningham, C.H.; Arai, T.; Yang, P.C.; Mc Connell, M.V.; Pauly, J.M.; and Conolly, S.M. (2005). Positive contrast magnetic resonance imaging of cells labelled with magnetic nanoparticles. *Magnetic Resonance in Medicine*, 53(5), 999-1005.

3. Johannsen, M.; Gneveckow, U.; Eckelt, L.; Feussner, A.; Waldofner, N.; Scholz, R.; Deger, S.; Wust, P.; Loening, S.A.; and Jordan, A. (2005). Clinical hyperthermia of prostate cancer using magnetic nanoparticles: presentation of a new interstitial technique. *International Journal of Hyperthermia*, 21(7), 637-647.
4. Freeman, M.W.; Arrott, A.; and Watson, J.H.L. (1960). Magnetism in medicine. *Journal of Applied Physics*, 31(5), S404-S405.
5. Kim, Y.-J.; Ebara, M.; and Aoyagi, T. (2013). A smart hyperthermia nanofiber with switchable drug release for inducing cancer apoptosis. *Advanced Functional Materials*, 23(46), 5753-5761.
6. Lengert, E.; Kozlova, A.; Pavlon, A.M.; Atkin, V.; Verkhovskii, R.; Kamyshinsky, R.; Demina, P.; Vasiliev, A.L.; Venig, S.B.; and Bukreeva, T.V. (2019). Novel type of hollow hydrogel microspheres with magnetite and silver nanoparticles. *Materials Science & Engineering: C*, 98, 1114-1121.
7. Yallapu, M.M.; Othman, S.F.; Curtis, E.T.; Bauer, N.A.; Chauhan, N.; Kumar, D.; Jaggi, M.; and Chauhan S.C. (2012). Curcumin-loaded magnetic nanoparticles for breast cancer therapeutics and imaging applications. *International Journal of Nanomedicine*, 7, 1761-1779.
8. Jain, T.K.; Richey J.; Strand, M.; Leslie-Pelecky, D.L.; Flask, C.; and Labhasetwar, V. (2008). Magnetic nanoparticles with dual functional properties: drug delivery and magnetic resonance imaging. *Biomaterials*, 29(29), 4012-4021.
9. Rahmawati, R.; Permana, M.G.; Harison, B.; Nugraha; Yuliarto, B.; Suyatman; and Kurniadi, D. (2017). Optimization of frequency and stirring rate for synthesis of magnetite (Fe_3O_4) nanoparticles by using coprecipitation-ultrasonic irradiation methods. *Procedia Engineering*, 170, 55-59.
10. Thommes, M.; Kaneko, K.; Neimark, A.V.; Olivier, J.P.; Rodriguez-Reinoso, F.; Rouquerol, J.; and Sing, K.S.W (2015). Physisorption of gases, with special reference to the evaluation of surface area dna pore size distribubtion (IUPAC Technical Report). *Pure Applied Chemistry*, 87(9-10), 1051-1069
11. Feczko, T.; Toth, J.; Dosa, G.; and Gyenis, J. (2011). Influence of process conditions on the mean size of PLGA nanoparticles. *Chemical Engineering and Processing: Process Intensification*, 50(8), 846-853.
12. Zhang, J.; Mei, Q.; Ding, Y.; Guo, K.; Yang, X.; and Zhao, J. (2017). Ordered mesoporous $NiCo_2O_4$ nanospheres as a novel electrocatalyst platform for 1-naphthol and 2-naphthol individual sensing application. *ACS Applied Materials and Interfaces*, 9(35), 29771-29781.
13. Nandiyanto, A.B.D.; Zaen, R.; and Oktiani, R. (2017). Correlation between crystallite size and photocatalytic performance of micrometer-sized monoclinic WO_3 particles. *Arabian Journal of Chemistry*, 13(1), 1283-1296.
14. Nandiyanto, A.B.D.; Oktiani, R.; Ragadhita, R.; Sukmafitri, A.; and Zaen, R. (2018). Amorphous content on the photocatalytic performance of micrometre-sized tungsten trioxide particles. *Arabian Journal of Chemistry*, 13(1), 2912-2924.
15. Nandiyanto, A.B.D.; Putra, Z.A.; Andika, R.; Bilad, M.R.; Kurniawan, T.; Zulhijah, R; and Hamidah, I. (2017). Porous activated carbon particles from rice straw waste and their adsorption properties. *Journal of Engineering*

Science and Technology (JESTEC), Special Issue on AASEC'2016, October, 1-11.

16. Mascolo, M.C.; Pei, Y.; and Ring, T.A. (2013). Room temperature co-precipitation synthesis of magnetite nanoparticles in a large pH window with different bases. *Materials*, 6(12), 5549-5567.
17. Goldberg, M.; Langer, R.; and Jia, X. (2007). Nanostructured materials for applications in drug delivery and tissue engineering. *Journal of Biomaterials Science, Polymer Edition*, 18(3), 241-268.
18. Rahmawati, R.; Kaneti, Y.V.; Taufiq A.; Sunaryo; Yuliarto, B.; Suyatman; Nugraha; Kurniadi, D.; Hossain M.S.A.; and Yamauchi, Y. (2018). Green synthesis of magnetite nanostructures from naturally available iron sands via sonochemical method. *Bulletin of Chemical Society of Japan*, 91(2), 311-317.
19. Bock, N.; Riminucci, A.; Dionigi, C.; Russo, A.; Tampieri, A.; Landi, E.; Goranov, V.A.; Marcacci, M.; and Dediu, V. A novel route in bone tissue engineering: Magnetic biomimetic scaffolds. *Acta Biomaterialia*, 6(3), 786-796
20. Bae, K.H.; Chung, H.J.; and Park, T.G. (2011). Nanomaterials for cancer therapy and imaging. *Molecules and Cells*, 31(4), 295-302.
21. Baldi, G.; Bonacchi, D.; Innocenti, C.; Lorenzi, G.; and Sangregorio, C. (2007). Cobalt ferrite nanoparticles: the control of the particle size and surface state and their effects on magnetic properties. *Journal of Magnetism and Magnetic Materials*, 311(1), 10-16.
22. Taufiq, A.; Sunaryono; Putra, E.G.R.; Okazawa, A.; Watanabe, I.; Kojima, N.; Pratapa, S.; and Darminto. (2015). Nanoscale clustering and magnetic properties of $Mn_xFe_{3-x}O_4$ particles prepared from natural magnetite. *Journal of Superconductivity and Novel Magnetism*, 28(9), 2855-2863.
23. Kazenimehaz, I and Mosivand, S. (2014). Phase transition of electrooxidized Fe3O4 to ϒ and α-Fe2O3 nanoparticles using sintering treatment. *Acta Physica Polonica Series A*, 125(5), 1210-1214.